◆ Human Brain Mapping 38:4613–4630 (2017) ◆

Spontaneous Activity in the Visual Cortex Is Organized by Visual Streams

Kun-Han Lu,[1,2] Jun Young Jeong,[1] Haiguang Wen,[1,2] and Zhongming Liu [1,2,3]*

[1]*School of Electrical and Computer Engineering, Purdue University, West Lafayette, Indiana*
[2]*Purdue Institute for Integrative Neuroscience, Purdue University, West Lafayette, Indiana*
[3]*Weldon School of Biomedical Engineering, Purdue University, West Lafayette, Indiana*

Abstract: Large-scale functional networks have been extensively studied using resting state functional magnetic resonance imaging (fMRI). However, the pattern, organization, and function of fine-scale network activity remain largely unknown. Here, we characterized the spontaneously emerging visual cortical activity by applying independent component (IC) analysis to resting state fMRI signals exclusively within the visual cortex. In this subsystem scale, we observed about 50 spatially ICs that were reproducible within and across subjects, and analyzed their spatial patterns and temporal relationships to reveal the intrinsic parcellation and organization of the visual cortex. The resulting visual cortical parcels were aligned with the steepest gradient of cortical myelination, and were organized into functional modules segregated along the dorsal/ventral pathways and foveal/peripheral early visual areas. Cortical distance could partly explain intra-hemispherical functional connectivity, but not interhemispherical connectivity; after discounting the effect of anatomical affinity, the fine-scale functional connectivity still preserved a similar visual-stream-specific modular organization. Moreover, cortical retinotopy, folding, and cytoarchitecture impose limited constraints to the organization of resting state activity. Given these findings, we conclude that spontaneous activity patterns in the visual cortex are primarily organized by visual streams, likely reflecting feedback network interactions. *Hum Brain Mapp 38:4613–4630, 2017.* © 2017 Wiley Periodicals, Inc.

Key words: fine-scale networks; independent component analysis; functional parcellation; visual streams

INTRODUCTION

Resting state functional magnetic resonance imaging (rs-fMRI) has been widely explored to map resting state networks (RSNs) that collectively report the brain's intrinsic functional organization (Fox and Raichle, 2007). These networks consist of temporally correlated regions (Biswal et al., 1995; Van Dijk et al., 2010), arise from structural connections (Honey et al., 2007; Van Den Heuvel et al., 2009), resemble and predict task activations (Cole et al., 2014; Smith et al., 2009; Tavor et al., 2016), and distinguish individual subjects (Finn et al., 2015) or diseases (Fox and Greicius, 2010). Although brain activity spans a variety of spatial scales (Doucet et al., 2011; Hutchison et al., 2013; Yoshimura et al., 2005), RSNs have been mostly characterized in the whole

Additional Supporting Information may be found in the online version of this article.

Contract grant sponsor: NIH; Contract grant number: R01MH104402; Contract grant sponsor: Purdue University.

*Correspondence to: Zhongming Liu, PhD, Assistant Professor of Biomedical Engineering, Assistant Professor of Electrical and Computer Engineering, College of Engineering, Purdue University, 206 S. Martin Jischke Dr., West Lafayette, IN 47907, USA.
E-mail: zmliu@purdue.edu

Received for publication 18 February 2017; Revised 5 June 2017; Accepted 7 June 2017.

DOI: 10.1002/hbm.23687
Published online 13 June 2017 in Wiley Online Library (wileyonlinelibrary.com).

brain, empirically and coarsely coined in terms of motor (Biswal et al., 1995), vision (Yeo et al., 2011), default-mode (Greicius et al., 2003), attention (Fox et al., 2006), salience (Seeley et al., 2007), and so on. In finer spatial scales, patterns of spontaneous activity and connectivity remain largely unclear, but may bear more specific functional roles related to perception, behavior, or cognition (Kenet et al., 2003; Lewis et al., 2016; Long et al., 2014; Wang et al., 2013; Wilf et al., 2017; Yoshimura et al., 2005).

In this regard, the visual cortex is a rich and ideal benchmark. It has been characterized in terms of cellular architectonics (Amunts et al., 2000; Glasser and Van Essen, 2011), structural connections (Felleman and Van Essen, 1991; Salin and Bullier, 1995), cortical folding (Benson et al., 2012; Fischl et al., 2008), functional pathways (Hubel and Wiesel, 1962; Ungerleider and Haxby, 1994), and neural coding (Guclu and van Gerven, 2015; Ohiorhenuan et al., 2010). In recent studies, correlation patterns of spontaneous activity in the visual cortex have been examined and compared with retinotopy (Arcaro et al., 2015; Bock et al., 2015; Butt et al., 2013; Dawson et al., 2016; de Zwart et al., 2013; Genc et al., 2016; Gravel et al., 2014; Heinzle et al., 2011; Jo et al., 2012; Lewis et al., 2016; Raemaekers et al., 2014; Striem-Amit et al., 2015; Wilf et al., 2017; Yeo et al., 2011). Since much of the visual cortex has visual-field maps-topographic representations of the polar angle and eccentricity (Wandell et al., 2007), it is reasonable to initially speculate that resting state activity is intrinsically organized by retinotopy. Support for this hypothesis comes in part from the finding that in early visual areas (e.g., V1–V3), correlations in spontaneous activity are generally higher between locations with similar eccentricity representations (Arcaro et al., 2015; Dawson et al., 2016; Genc et al., 2016; Gravel et al., 2014; Heinzle et al., 2011; Jo et al., 2012; Lewis et al., 2016; Striem-Amit et al., 2015; Yeo et al., 2011). However, such eccentricity-dependent functional connectivity has rarely been reported beyond early visual areas (Baldassano et al., 2013; Striem-Amit et al., 2015); it may be relatively weak (Wilf et al., 2017) or observable only after regressing out large-scale activity (Raemaekers et al., 2014), and may also be confounded by the decay of local connectivity over cortical distance (Butt et al., 2013; Dawson et al., 2016). Further against this hypothesis, spontaneous activity preserves little or less polar-angle dependence in intrahemispheric correlations (Bock et al., 2015; Gravel et al., 2014; Wilf et al., 2017), and shows strong correlations between bilateral V1 locations despite their lack of common receptive fields or direct connections (de Zwart et al., 2013; Jo et al., 2012). As such, the retinotopic organization of fine-scale resting activity in the visual cortex may be questionable (Butt et al., 2013; Wilf et al., 2017). It is likely that the apparently eccentricity-dependent spontaneous activity and connectivity might reflect alternative representations that partly overlap with the eccentricity representation in early visual areas, as opposed to retinotopy per se.

In fact, cortical representations of the peripheral and central visual fields partly overlap with the magnocellular and parvocellular streams (Nassi and Callaway, 2009; Schiller et al., 1990), and extend onto the dorsal and ventral pathways for visual action and perception, respectively (Goodale and Milner, 1992; Ungerleider and Haxby, 1994). Along these pathways, feedforward neuronal circuits convey and integrate not only visual positions, but also increasingly complex visual or conceptual features (Hasson et al., 2008; Martin, 2007; Yamins and DiCarlo, 2016). Top-down feedback connections are not or less retinotopically organized than are feedforward pathways (Salin and Bullier, 1995). The complex interplay between feedforward and feedback processes is essential for natural vision (Gilbert and Li, 2013; Rao and Ballard, 1999), but remains largely unclear in a stimulus-free resting state. Thus, spontaneously emerging networks in the visual cortex may not readily fit the retinotopic organization, or arguably any other presumable organizations.

What is needed is a data-driven analysis of resting-state activity in a finer spatial scale, unbiased by any presumed areal definition or organizational hypothesis. For this purpose, independent component analysis (ICA) is well suited but has not been applied to finer spatial scales, to our knowledge, despite its wide application to whole-brain fMRI signals (Damoiseaux et al., 2006). Unlike the correlation analysis (Baldassano et al., 2012; Genc et al., 2016), ICA also has the advantages of being multivariate and data-driven, thereby bypassing the potential bias from any narrowly-focused hypothesis (Calhoun et al., 2009). Here, we explored a new application of ICA for mapping cortical visual areas and networks based on rs-fMRI signals within the visual cortex. In this sub-system scale, the fine-grained activity patterns derived from ICA were systematically characterized, interpreted, and evaluated for their test-retest reproducibility and individual variations. Moreover, they were also compared against cortical folding (Destrieux et al., 2010), retinotopy (Abdollahi et al., 2014), cytoarchitecture (Van Essen et al., 2012a), myeloarchitecture (Glasser et al., 2014), and the latest multimodal cortical parcellation (Glasser et al., 2016). Clustering analysis further reveals that spontaneously emerging network patterns in the human visual cortex may not be retinotopically organized; instead, they are temporally clustered into four modules: the dorsal pathway, the ventral pathway, and the foveal and peripheral subdivisions of early visual areas.

MATERIALS AND METHODS

Subjects and Data

We used the rs-fMRI data released from the Human Connectome Project (HCP) (Van Essen et al., 2013). Briefly, we randomly selected 201 independent healthy subjects; for each subject, we used the data from two resting state

sessions (session 1 for test and session 2 for retest); each session was 14 min and 33 s with the eyes open and fixating.

As elaborated elsewhere (Van Essen et al., 2012b), data were acquired in a 3-tesla MRI system with a 32-channel head coil (Skyra, Siemens, Germany). The rs-fMRI data we used were acquired with a single-shot, multiband-accelerated, gradient-recalled echo-planar imaging with nominally 2 mm isotropic spatial resolution and 0.72 s temporal resolution, and left-to-right phase-encoding. In addition, structural images with T_1 and T_2-weighted contrast were both acquired with 0.7mm isotropic resolution.

As elaborated elsewhere (Glasser et al., 2013), the structural images were nonlinearly registered to the Montreal Neurological Institute (MNI) template, where the images were combined and segmented to generate cortical surfaces. The fMRI images were corrected for slice timing and motion, aligned to structural images, normalized to the MNI space, projected onto the cortical surfaces, and coregistered across subjects. In addition to the minimal preprocessing described above, we removed the slow trend in the fMRI time series by regressing out a fourth-order polynomial function, and subtracted the mean and standardized the signal variance. Note that we did not subtract or regress out the "global" signal either averaged across the whole brain or the visual cortex. Neither was spatial smoothing performed in order to minimize spurious correlations in neighboring voxels.

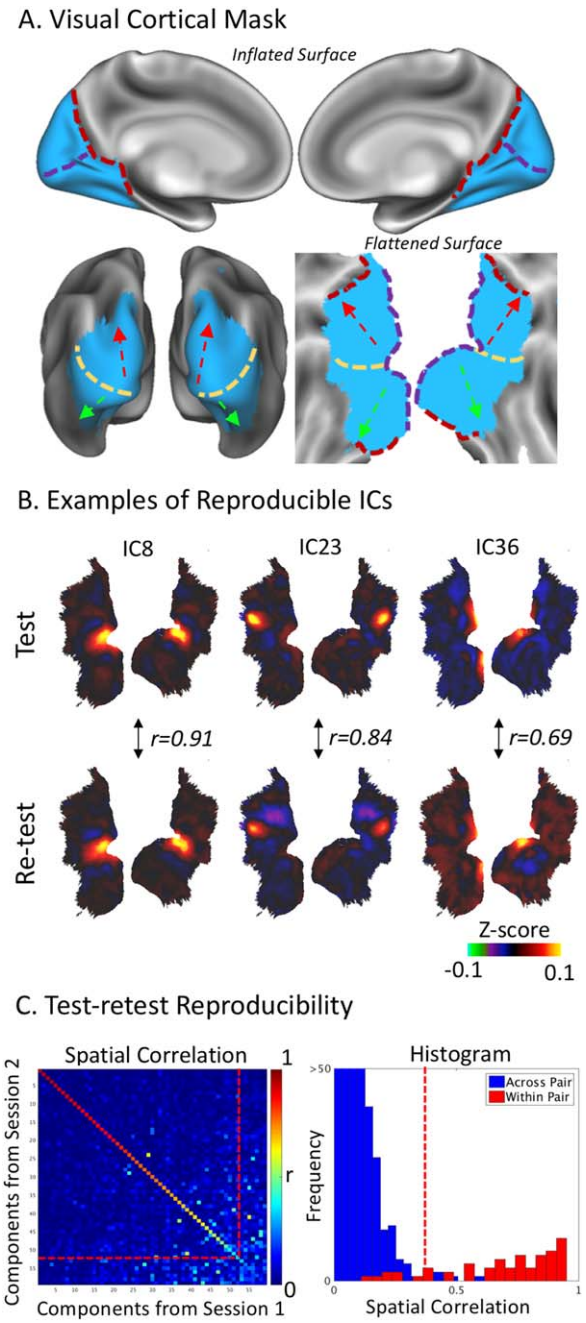

IC Analysis

We applied the ICA to the rs-fMRI signals within a mask of the visual cortex (Fig. 1A), defined by a system-level functional parcellation of the human cortex (Yeo et al., 2011). The fMRI time series within the mask was temporally standardized (i.e., subtracting the mean and standardizing the variance) and concatenated across subjects. Infomax ICA (Bell and Sejnowski, 1995) was used to decompose the concatenated rs-fMRI data into 59 spatially ICs within the visual cortex. Here, the number of ICs, 59, was determined by maximizing the Laplace approximation of the posterior probability of the ICA model order (Beckmann and Smith, 2004). The spatial pattern of each component was converted to a z-score map by dividing the IC weight at each voxel by the standard deviation of the

Figure 1.

Visual cortical mask and reproducibility of fine-scale network patterns. **A**: The visual cortex mask (in blue) is illustrated on inflated and flattened cortical surfaces. Reference lines mark the occipital-parietal sulcus (red dash line), the calcarine sulcus (purple dash line), a rough ventral-dorsal division (yellow dash line), from where the ventral and dorsal pathways are along the green and red arrows, respectively. **B**: Three examples of reproducible ICs that exhibit high correlations (r) in their spatial patterns. The color scale represents the z-score and is ranged from −0.1 to 0.1. **C**: The left panel shows the spatial correlation matrix between the ICs obtained from two repeated resting-state sessions. The diagonal elements correspond to uniquely paired ICs; the off-diagonal elements are between unpaired ICs. The red line represents a correlation threshold ($r = 0.4$), by which a pair of ICs was considered reproducible between sessions. The right panel shows the discrete histograms of the correlations for the paired (red) and unpaired (blue) ICs. [Color figure can be viewed at wileyonlinelibrary.com]

voxel-wise residual noise that could not be explained by the ICA model (Beckmann and Smith, 2004). The spatial IC maps were visualized in terms of color-coded z-scores.

Test-Retest Reproducibility

Furthermore, we evaluated the test-retest reproducibility of the ICA results. In a group level, the ICA applied to the data in one session (i.e., session 1) was also applied to the data in a repeated session (i.e., session 2); both sessions were from the same group of subjects, and the data was concatenated in the same order across subjects. We calculated the absolute value of the spatial correlation (r) between every component from session 1 and every component from session 2, and paired these components across sessions into distinct pairs to maximize the sum of their absolute spatial correlations. More specifically, we used an iterative procedure toward the optimal pairing: we began with identifying a pair of ICs (one from session 1, and the other from session 2) with the highest correlation, and paired these two ICs; then, we excluded the paired ICs from subsequent pairing, which continued until all ICs were paired. Note that the absolute spatial correlation was used since a reproducible IC could show the same spatial distribution despite opposite polarity. A threshold ($|r| \geq 0.4$) was used to identify reproducible components for further interpretation (Fig. 1C). Our focus on reproducible components was given an assumption: resting-state activity patterns that report the functional organization are more reproducible and reliable within and across subjects than noise.

We also explored the potential confounding effects of head motion on fine-scale ICs. For each subject, we regressed out the time series of six motion correction parameters prior to group-level ICA. We compared the ICs obtained without and with the above motion correction, and further identified and excluded those ICs that appeared inconsistent solely due to this preprocessing step.

Modularity Analysis

For all the ICs that were reproducible and unaffected by head motion correction, we computed the temporal correlations between different components. Such correlations were first calculated based on component time series from each subject, and then averaged across subjects. This procedure prevented the resulting correlations from being dominated or biased by intersubject variations. To evaluate the statistical significance of the between-component correlation, we converted the correlation coefficient to the z-score (using the Fisher's r-to-z transform) separately for each subject, and then applied a one-sample t-test to the z-scores from all the subjects (with dof = 200 and the significance level at 0.01 with Bonferroni correction for the number of voxels).

We also applied the Louvain modularity analysis (Blondel et al., 2008) to the cross-component correlation matrix averaged across subjects. It assigned individual ICs to different modules, such that the temporal correlations were higher within every module but lower between modules. The modularity analysis, including the determination of the number of modules, was based on the algorithm (a Matlab function: *modularity_louvain_und_sign*) implemented in Brain Connectivity Toolbox (Rubinov and Sporns, 2010). The modularity index, Q, was calculated to quantify the goodness of modularity partitions (ranging from 0 to 1). To evaluate the statistical significance of Q, we randomly shuffled the values in the correlation matrix 10,000 times and computed Q for each permutation given the same module assignment. This generated a null distribution of Q, against which the p value was computed for the Q value without permutation. To visualize the modular organization on the cortical surface, we represented each IC by a sphere located at the peak location in the component map, and color-coded every IC by its module membership.

Modeling and Discounting the Effect of Cortical Distance

The effects of cortical distance on fine-scale functional connectivity and its organization were evaluated and discounted as the following. For every pair of voxels within the same hemisphere of the visual cortex, their temporal correlation (converted to the z-score, z, by the Fisher's z transformation) was plotted and modeled as a function of their geodesic cortical distance, d (using the "-surface-geodesic-distance" function in HCP). As previously explored elsewhere (Honey et al., 2009), the distance to correlation relationship was fitted with a rational function ($z = c/d$), where the coefficient c was determined by least-squares estimations (using the "fitnlm" function in Matlab). Note that interhemispherical correlation was not modeled by distance, as the cortical distance between locations from different hemispheres was assumed to be infinite.

Next, we identified the peak location in each component map (hereafter referred to as the component centroid). For bilaterally distributed components, two centroids were identified, one at each hemisphere. The cortical distances between component centroids were computed for each hemisphere and each subject, and then averaged across subjects. The functional connectivity between ICs that could be explained by their anatomical distance, namely the distance-modeled functional connectivity, was quantified using the distance-to-correlation model as aforementioned. The distance-modeled functional connectivity matrix was subtracted from the original between-component functional connectivity matrix, yielding a residual functional-connectivity matrix that discounted the distance effect. Modularity analysis was then applied to the residual matrix. The resulting modular organization

was visualized on the cortical surface in the same way as aforementioned in the previous section, for a direct comparison between the modular organization of functional connectivity with and without discounting the effect of anatomical affinity.

Intrinsic Functional Parcellation of the Visual Cortex

From all the ICs, we created a group-level intrinsic functional parcellation of the visual cortex with an increasing level of granularity. Specifically, we defined a feature vector for each voxel in the visual cortex. This feature entails the weights by which the individual time series of different ICs were linearly combined to explain the fMRI signal observed at each voxel. Then we grouped the cortical voxels into distinct parcels by applying the *k*-means clustering to the corresponding feature vectors using a correlation-based "distance" and 1,000 replications with random initialization. The number of clusters (k) was empirically set to 10, 20, 30, and 40. The parcels were sequenced in an ascending order of the average correlation within each parcel, and were color-coded from 0 to 1 with equal spacing. We preferred this *k*-means clustering analysis to a "winner-take-all" alternative, in which each voxel was assigned to only one IC with the greatest weight (among all the ICs) at the given voxel. This was because single voxel time series were not necessarily represented by only one IC, but instead often by multiple ICs.

To facilitate interpretation, the ICA components and the parcellation derived from them were compared against conventional visual areas or cortical parcellation based on various structural and/or functional properties, including myeloarchitecture (Glasser et al., 2014), cytoarchitecture (Eickhoff et al., 2005), cortical folding (Destrieux et al., 2010), retinotopic mapping (Abdollahi et al., 2014), and multimodal parcellation (Glasser et al., 2016).

Dual-Regression and Individual-Level Parcellation

Following group ICA, we also used dual regression against each subject's fMRI data to characterize subject-specific ICA maps (Tavor et al., 2016). Briefly, we first applied multiple regression to the spatial domain, using the group-level ICA spatial maps as a set of spatial regressors to obtain individual-level time series that was associated with each group-level spatial map based on the subject-specific fMRI data; after normalizing these individual-level time series to a zero mean and a unitary variance, we applied multiple regression to the time domain, by using the normalized individual-level time series as temporal regressors to obtain the subject-specific ICA spatial maps. Intersubject reproducibility was evaluated separately for each IC as its spatial correlation across subjects. From the individual-level ICA maps, we also used the *k*-means clustering analysis ($k = 40$), as mentioned above, to create the visual-cortex parcellation specific to each subject. The similarity between subject-wise parcellations and the group-level parcellation was quantified with the Dice Similarity Coefficient (DSC; Shen et al., 2013). DSC measures the percentage of spatial overlap between a group-level parcel and its counterpart in each subject. The DSC ranged from 0 to 1 (one for exact overlap, whereas zero for no overlap at all). For each group-level parcel, its DSC was averaged across all subjects. The averaged DSC was displayed and compared across different parcels.

RESULTS

Intrinsic Activity Patterns within the Visual Cortex

Here, we explored a data-driven analysis of spontaneous activity confined to the human visual cortex. In this finer subsystem scale, our goal was to characterize and map intrinsic activity patterns to delineate cortical visual areas and networks independent of any task context or any presumed organizational hypothesis. Towards this goal, we used a cortical mask (Fig. 1A), based on a systems-level parcellation of the entire cortex (Yeo et al., 2011), to only select rs-fMRI activity within the human visual cortex for group ICA. The selected rs-fMRI data from 201 healthy human subjects in the HCP were temporally standardized within each subject and concatenated across subjects. The concatenated data were then decomposed into 59 spatially ICs. Repeating this analysis with data from a different resting-state session for the same subjects allowed us to evaluate the test-retest reproducibility of every component. For example, Figure 1B displays three typical ICs that were spatially consistent (or correlated) between the two repeated sessions. By pairing the ICs across sessions to maximize the sum of the absolute pairwise correlation coefficients, we identified 50 unique pairs of reproducible components, which showed higher spatial correlations within pairs ($|r| > 0.4$, mean $\pm$ S.D $= 0.78 \pm 0.14$) than across pairs (mean $\pm$ S.D $= 0.04 \pm 0.05$; Fig. 1C). In addition, we found that IC51 and IC55 yielded high spatial correlations with IC36 ($r = 0.578$) and IC41 ($r = 0.63$), respectively; they were not paired by the pairing algorithm, because IC36 and IC41 were better paired with other components while the pairing algorithm did not allow any duplication. Nevertheless, we included IC51 and IC55 as reproducible components in subsequent analyses. These results suggest that the ICA-derived spontaneous activity patterns are robust and reproducible in a subsystem spatial scale.

Figure 2 shows the spatial maps of all 52 reproducible components in a descending order of their test-retest reproducibility. Among them, 92% showed focal patterns, and fewer ICs were distributed (IC#: 34, 35, 49, 50); 30% showed bilateral distributions (IC#: 4, 8, 17, 19, 23, 28, 30, 31, 33, 34, 35, 36, 46, 49, 50); 36% showed clearly anti-

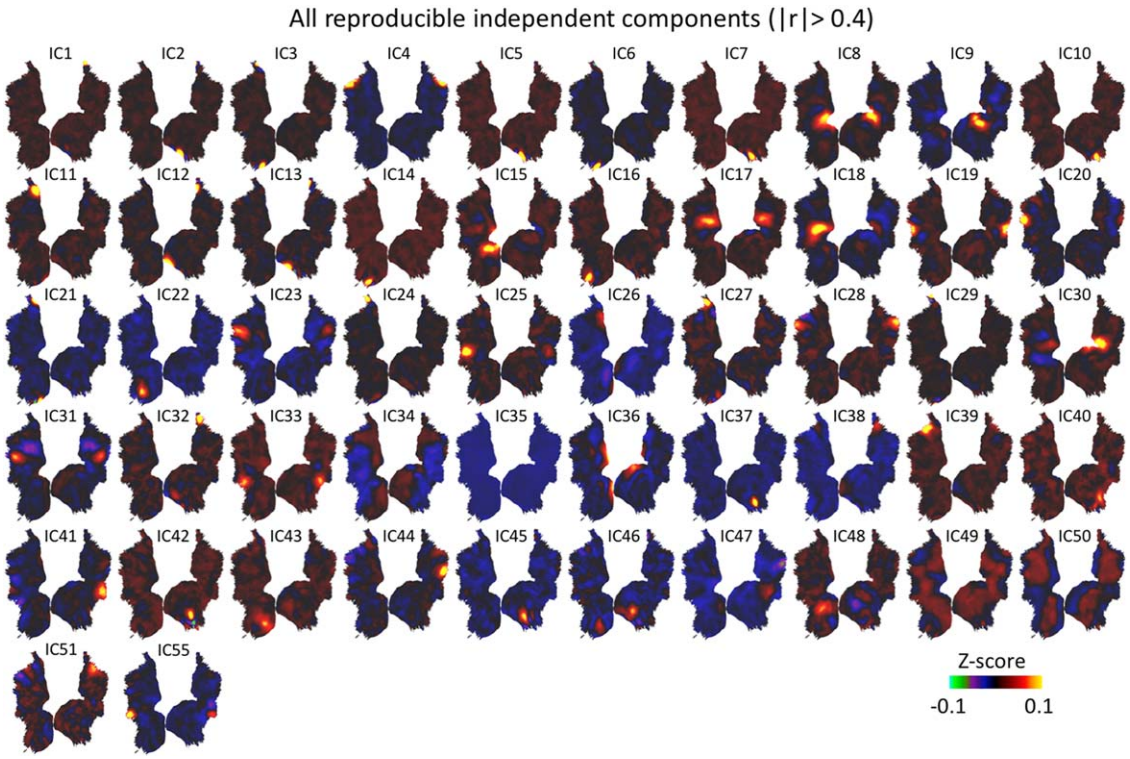

Figure 2.

Fifty-two reproducible ICs with spatial correlation >0.4. The ICs were numbered in a descending order of their test-retest reproducibility. IC51 and IC55 were not optimally matched by our algorithm, but they yielded spatial correlations of 0.58 and 0.63 with IC39 and IC41 respectively. Therefore, they were also considered to be reproducible. [Color figure can be viewed at wileyonlinelibrary.com]

correlated patterns with well localized positivity and negativity (IC#: 2, 3, 5, 6, 7, 8, 13, 15, 17, 21, 27, 29, 30, 31, 34, 42, 49, 50). Some of these components not only aligned with existing anatomical borders (e.g., IC36 and IC50 aligned with V1/V2 border), but also aligned with regions with known functional properties (e.g., IC41 and IC55 both matched well with the region MT).

Next, we attempted to identify the components that might be susceptible to artifacts related to head motion. We compared the ICs obtained without and with motion correction (i.e., regressing out head motion correction parameters from voxel time series). Among all the components shown in Figure 2, three ICs (IC34, IC49, IC50) with distributed patterns did not match to any of the ICs ($|r| < 0.15$) obtained after motion correction (Supporting Information Fig. S1A). Thus, we attributed these ICs to head motion, and further excluded them from subsequent analyses. All other 49 ICs in Figure 2 were one-to-one matched to the ICs after head motion correction, showing high spatial correlations for all matched pairs (Supporting Information Fig. S1B). In the following sections, we further segregated and interpreted these 49 ICs by comparing them to existing visual areas or networks.

Comparing Discrete ICA Components with Existing Visual Areas

Since the ICA-derived activity patterns mostly showed discrete regions with well-defined borders (Fig. 2), we further compared such discrete ICs with the visual areas defined with a recently published multi-modal parcellation (MMP; Glasser et al., 2016). For the primary visual area (V1), four components were found to be sharply confined to V1 (Fig. 3A). IC8 matched the bilateral foveal representations in V1; IC36 also showed bilateral distributions and corresponded to more peripheral representations; IC26 and IC38 showed unilateral distributions, corresponding to the most peripheral part of the right and left visual fields, respectively; these components did not overlap each other and all aligned with the V1 border. Therefore, V1 consists of multiple intrinsic functional sub-divisions apparently organized according to eccentricity representations, being largely symmetric not only between the left and right hemispheres, but also between the upper and lower sides of the calcarine sulcus. Unlike V1, V2 or V3 did not confine any component within itself. Instead, multiple components spanned across V2 and V3 along either

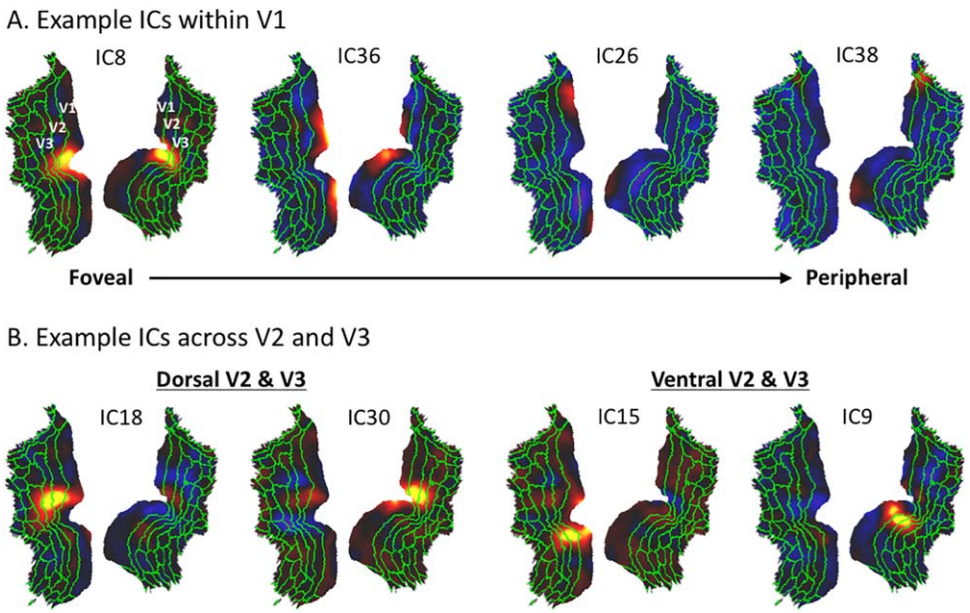

Figure 3.
Discrete ICs within the early visual areas (V1/V2/V3). **A**: Four ICs within V1. **B**: Four ICs across V2 and V3. The green lines are the borders of the MMP (Glasser et al., 2016), where V1/V2/V3 are defined. [Color figure can be viewed at wileyonlinelibrary.com]

the dorsal (IC18, IC30) or ventral (IC15 and IC9) direction (Fig. 3B). Compared to those components within V1, the V2/V3 components were less bilaterally symmetric; none of them included regions in both dorsal and ventral pathways.

Beyond those in early visual areas (V1/V2/V3), other discrete components were all anatomically split by the dorsal-ventral division. In the dorsal pathway, some components matched well with existing visual areas (Fig. 4A), including the middle temporal (MT: IC41 on the right hemisphere, IC55 on the left hemisphere), caudal area of inferior parietal cortex (PGp: IC19), dorsal visual transitional area (DVT: IC51 on the right hemisphere, IC39 on the left hemisphere) and parieto-occipital sulcus area 2 (POS2: IC4). Some other components were distributed across multiple visual areas, including the third visual area and the area intraparietal 0 (V3B/IP0: IC44 on the right hemisphere, IC20 on the left hemisphere), third visual areas and the fourth visual area (V3A/V3B/V3CD/V4: IC31), the dorsal visual transitional area and the sixth visual area (DVT/V6A: IC28), and the third visual area, the sixth visual area and the seventh visual area (V3A/V6A/V7: IC23); about half of these dorsal components were bilaterally symmetric. Along the ventral pathway, the majority of the components covered multiple visual areas (Fig. 4B), including ventral-medial visual areas (VMV1/VMV2/VMV3: IC42 on the right hemisphere, IC22 on the left hemisphere), para-hippocampal areas (PHA2/PHA3: IC10 on the right hemisphere, IC16 on the left hemisphere), fourth visual areas and the area lateral occipital 2 (V4t/LO2: IC33), the ventral visual complex and the fusiform face complex (VVC/FFC: IC40), except for VMV1 (IC45); only two ventral components were bilaterally symmetric; the rest of them were lateralized.

Functional Modularity in the Visual Cortex

For all discrete components, we further evaluated their modular organization based on their temporal correlations. The between-component correlation matrix was calculated for every subject, and then averaged across subjects. The resulting group-level correlation matrix was re-organized into four functional modules based on the Louvain modularity analysis (Blondel et al., 2008; Rubinov and Sporns, 2010). Components within the same module were strongly and positively correlated, whereas components from different modules were weakly or negatively correlated (Fig. 5B, left). Visualizing the distributions of these functional modules on the cortical surface revealed their anatomical segregation (Fig. 5A). As each unilateral (or bilateral) component was represented by one sphere (or two spheres), the first module included components over the foveal representations of early visual areas (V1, V2, and V3); the second module was mostly distributed over the peripheral representations of early visual areas; the third module was distributed along the dorsal pathway; the fourth module was distributed along the ventral pathway (Fig. 5A). The modularity index ($Q = 0.4966$) was statistically significant ($P < 0.0001$, nonparametric permutation test). The between-component correlations within every module were

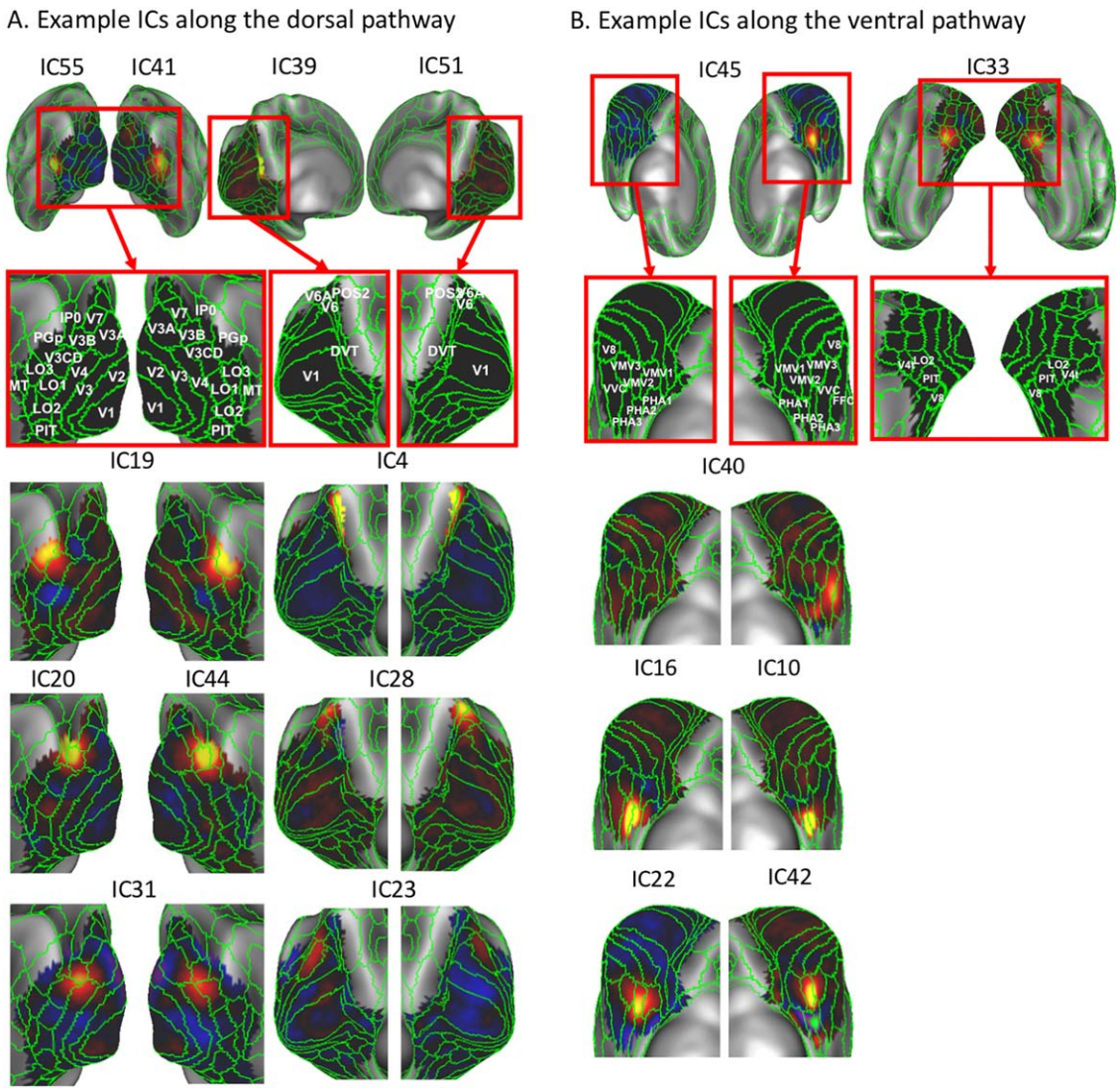

Figure 4.

Discrete ICs along the dorsal pathway and ventral pathway. **A**: The left panel shows the ICs that match well with existing lateral visual areas in the dorsal pathway. The right panel shows the ICs that match well with existing medial visual areas in the dorsal pathway. **B**: Example ICs that match well with existing medial visual areas in the ventral pathway such as VMV1–3, FFC, and VVC. The green lines mark the existing visual areal borders according to the MMP. For the sake of illustration, unilaterally distributed ICs (i.e., IC55 and IC41 at left and right MT, respectively) are shown together in one panel. [Color figure can be viewed at wileyonlinelibrary.com]

consistently high for most of the subjects, yielding high t statistics, especially for the module at foveal early visual areas and the module at higher-order ventral visual areas. The t statistics corresponding to the correlations across different modules were mostly low and not significant. These results lend support to the notion that intrinsic networks within the visual cortex are organized into functional modules: the dorsal pathway, the ventral pathway, as well as the foveal and peripheral parts of the early visual areas.

Effects of Cortical Distance on Functional Connectivity and Modularity

However, the above functional modules were anatomically clustered. This observation led us to ask whether the functional relationships between individual ICs were entirely attributable to their cortical distances. To address this question, we modeled the temporal correlations within the visual cortex as a function of the cortical distance between voxels, separately evaluated for each hemisphere.

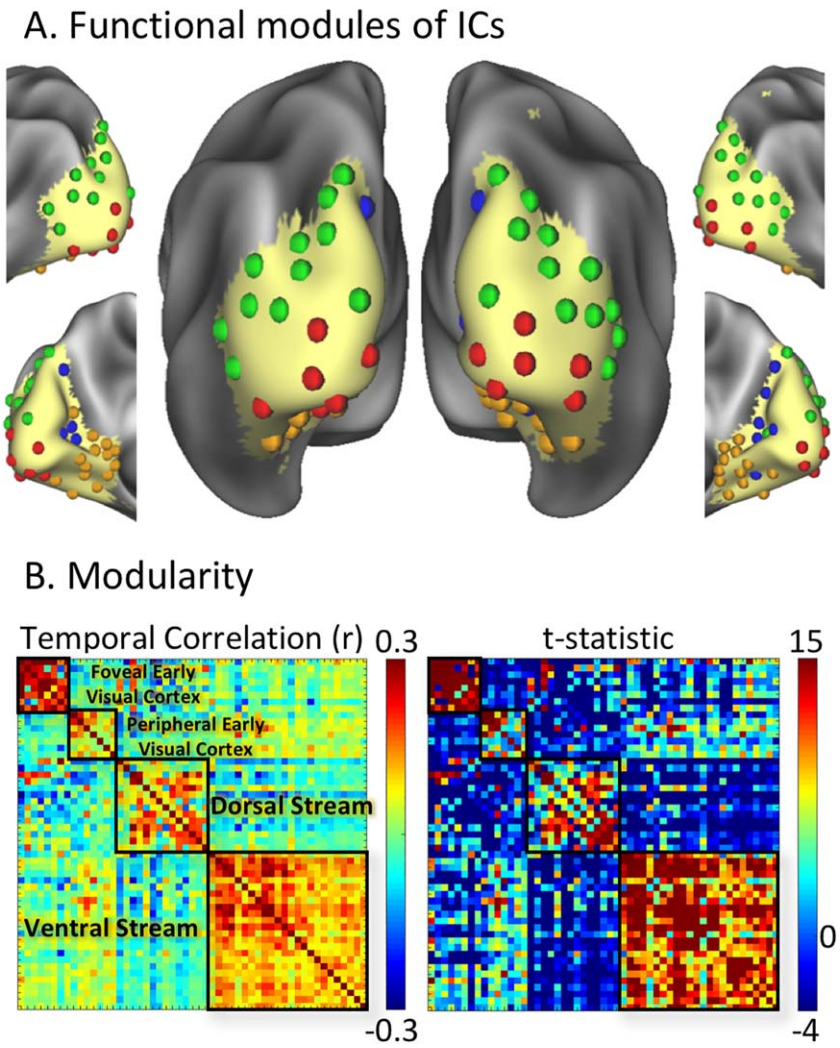

Figure 5.

Functional modules in the visual cortex. **A**: Each component is represented with a sphere, colored coded by its modular membership, and placed at the peak location of its spatial map. **B**: The matrix on the left shows the temporal correlations (r) between ICs, organized into four modules [in (1) foveal early visual cortex, (2) peripheral early visual cortex, (3) dorsal pathway, (4) ventral pathway]. The matrix on the right shows the t-statistics associated with the temporal correlations (z) between ICs, organized in the same order as the correlation matrix on the left. [Color figure can be viewed at wileyonlinelibrary.com]

The scatter-plot of correlation (z) versus distance (d) revealed a reciprocal relationship between them. This relationship was thus modeled as $z = 64.617/d$, based on nonlinear least-squares estimation (Fig. 6A; $P < 0.00001$). It suggests that fine-scale functional connectivity within a cortical hemisphere depends, at least in part, on cortical distance, in line with findings from previous studies (Dawson et al., 2016; Genc et al., 2016).

We further asked whether the modular organization based on functional connectivity (Fig. 5) could be entirely attributed to spatial affinity given the apparent reciprocal (distance-to-correlation) relationship (Fig. 6A). To address this question, we computed the cortical distances between component centroids separately for each hemisphere (Fig. 6B), and then estimated their effects on functional connectivity based on the distance-to-correlation model (Fig. 6C). To evaluate the distance-dependent connectivity, Figure 6D shows the original between-component functional connectivity organized by the same modular memberships as in Figure 5B, but separated by hemispheres. As shown in Figure 6E, the residual matrix after subtracting Figure 6C from 6D represented the functional connectivity after discounting the effect of cortical distance. Applying the modularity analysis to this residual matrix (Fig. 6E) revealed a similar modular organization (Fig. 6F) as was obtained with the original functional connectivity matrix (Fig. 5B). Specifically, five

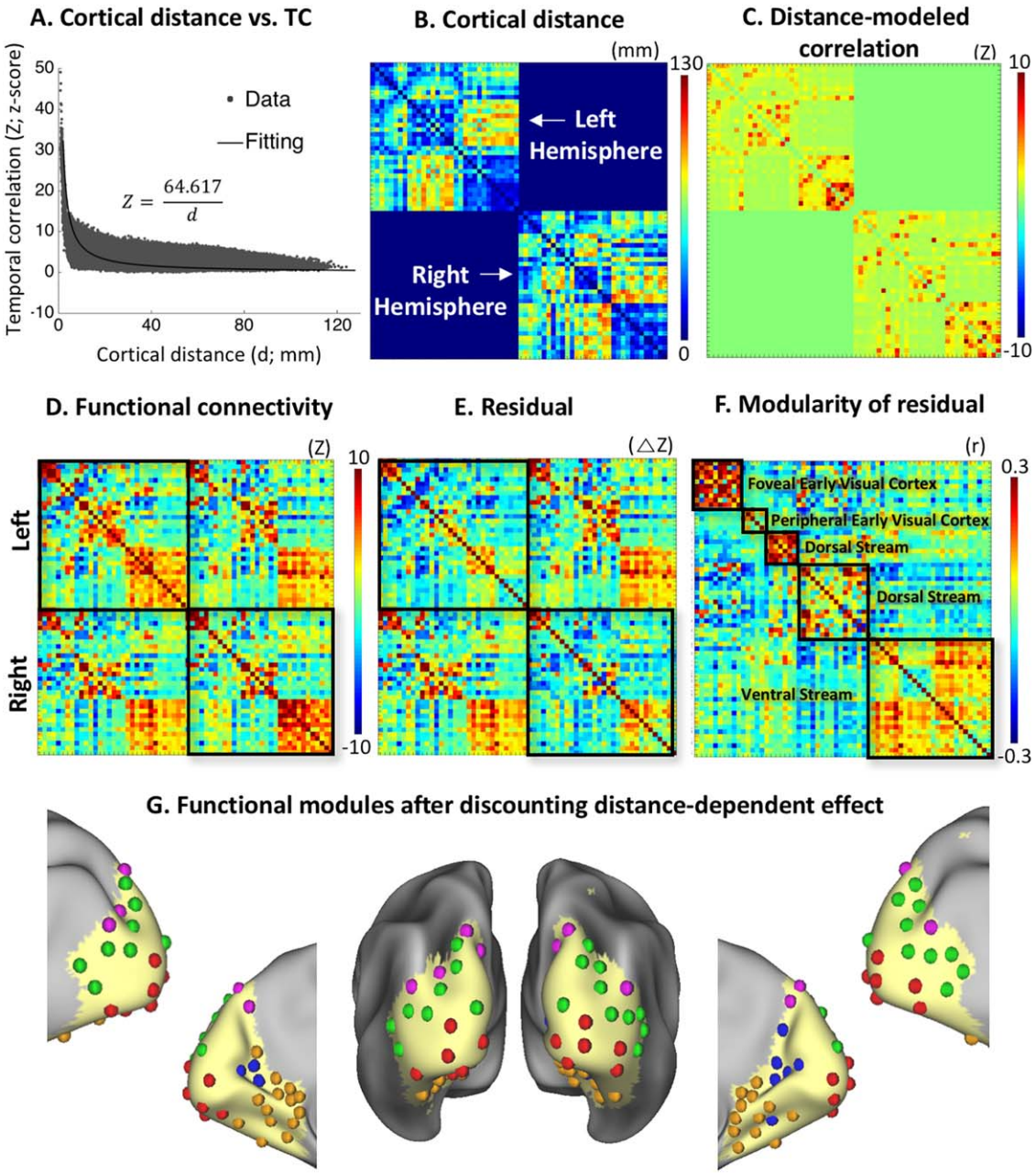

Figure 6.

The effect of cortical distance on functional connectivity and modularity. **A**: The scatter-plots of correlation (z) vs. distance (*d*), which were modeled as $z = 64.617/d$ based on least-squares estimation. The intrahemispheric correlations from both hemispheres were plotted and used for model fitting. **B**: The matrix shows the cortical distances between component centroids separately for each hemisphere. **C**: The correlations between components as modeled by the distances between component centroids. **D**: The between-component functional connectivity organized by the same modular memberships as in Figure 5B, but separated by hemispheres (in z-score). **E**: The residual matrix after subtracting Figure 6C from 6D, representing the functional connectivity after discounting the effect of cortical distance. **F**: Modular organization of the residual matrix showing five modules. **G**: Each component is represented with a sphere, colored coded by its modular membership in the panel F, and placed at the peak location of its spatial map. [Color figure can be viewed at wileyonlinelibrary.com]

functional modules were observed after discounting the distance effect: two for the foveal and peripheral representations in early visual areas, one in the ventral pathway, and two in the dorsal pathway (Fig. 6G). The modularity index (Q) was 0.6095 and statistically significant ($P < 0.01$, nonparametric permutation test). The spatial distribution of each module was generally similar either with or without discounting the distance effect, except that the dorsal-stream module was divided into two modules after the distance effect was mathematically removed. These results suggest that spontaneous functional connectivity in the visual cortex reveals a robust modular organization and distribution that are partly dependent on, but not entirely attributed to, the anatomical affinity between cortical locations or areas.

Functional Parcellation of the Visual Cortex

Following ICA, we applied the k-means clustering to the ICA feature vector (the weights by which the individual time series of different ICs were linearly combined to explain the fMRI signal) at every voxel within the visual cortex, yielding an automated intrinsic parcellation of the visual cortex with a varying level of granularity with the number of clusters (k) being 10, 20, 30, and 40. As such, voxels that entailed more similar feature vectors were more likely to be grouped into the same cluster. We found that as the number of clusters increased, coarser parcels were progressively subdivided into finer parcels (Fig. 7). We settled at $k = 40$, which roughly matched the expected number of visual areas (Glasser et al., 2016), and generated a set of well-defined and bilaterally symmetric parcels (Fig. 8). This parcellation based on spontaneous activity was further compared against existing parcellations of the visual cortex, based on the whole-brain multimodal images (i.e., MMP; Glasser et al., 2016), visual-field maps (Abdollahi et al., 2014), cortical folding patterns (Destrieux et al., 2010), cortical cytoarchitecture (Eickhoff et al., 2005), and cortical myelination (Glasser et al., 2014). It was found that none of the existing parcellations precisely agreed with the fully automated and data-driven parcellation reported here. In particular, our parcellation did not match with those based on cortical retinotopy, cytoarchitecture, and folding, but matched relatively better with the cortical myelination and the MMP. In our parcellation, the outer contour of cortical parcels that covered early visual areas tended to align well with the steep gradients of cortical myelination. Our reported cortical parcels that covered the high-level visual areas tended to align reasonably well with the corresponding parcels in MMP, although the alignment was not one to one. Compared with MMP, our parcellation was coarser in high-level visual areas, but finer in low-level visual areas.

Parcellation in the Level of Single Subjects

In addition to the group-level analysis, we also applied dual regression to the data from every subject in an attempt to obtain the corresponding ICA patterns for individual subjects. The individual-level ICA patterns were comparable with the group-level ICA patterns (Fig. 9A), and were spatially correlated between different subjects (r; mean ± S.D = 0.46 ± 0.08; Fig. 9B). On the basis of individual-specific ICs, the visual cortex was parcellated ($k = 40$) for each subject (see examples in Fig. 9C, left). The individualized parcels were relatively noisy but generally consistent to the group-level parcellation. To visualize the consistency across individuals, each group-level parcel was assigned with a DSC, indicating its spatial overlap with the corresponding parcels in individual subjects. For all different parcels, the DSC ranged from 0.27 to 0.76 with an average of 0.58, suggesting reasonably high intersubject reproducibility. However, the reproducibility varied across parcels (Fig. 9C, right). The most reliable parcels tended to be higher-order visual areas.

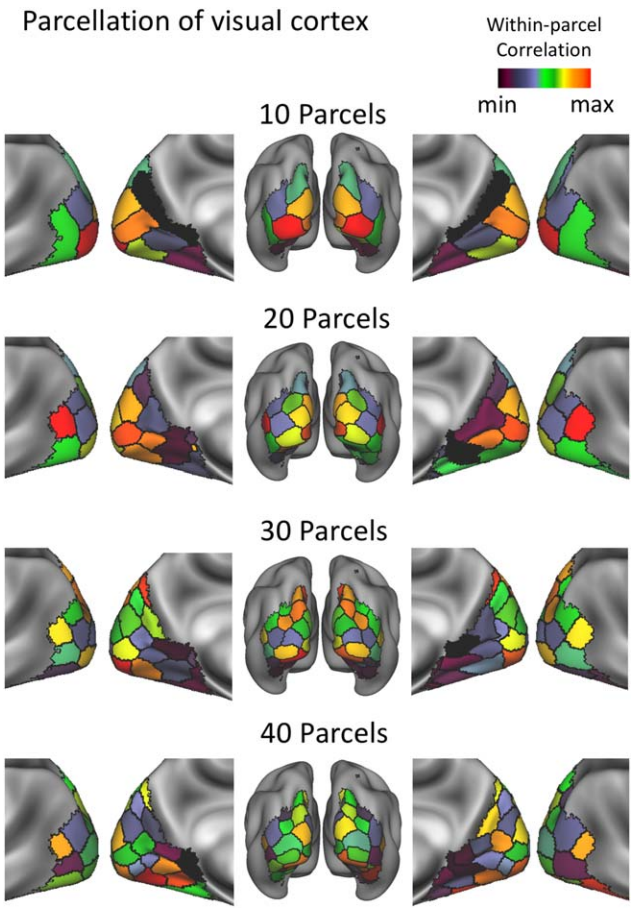

Figure 7.
Functional parcellation of the visual cortex with a varying number of parcels (k = 10, 20, 30, and 40). The parcels were color-coded according to the averaged within-parcel correlation. [Color figure can be viewed at wileyonlinelibrary.com]

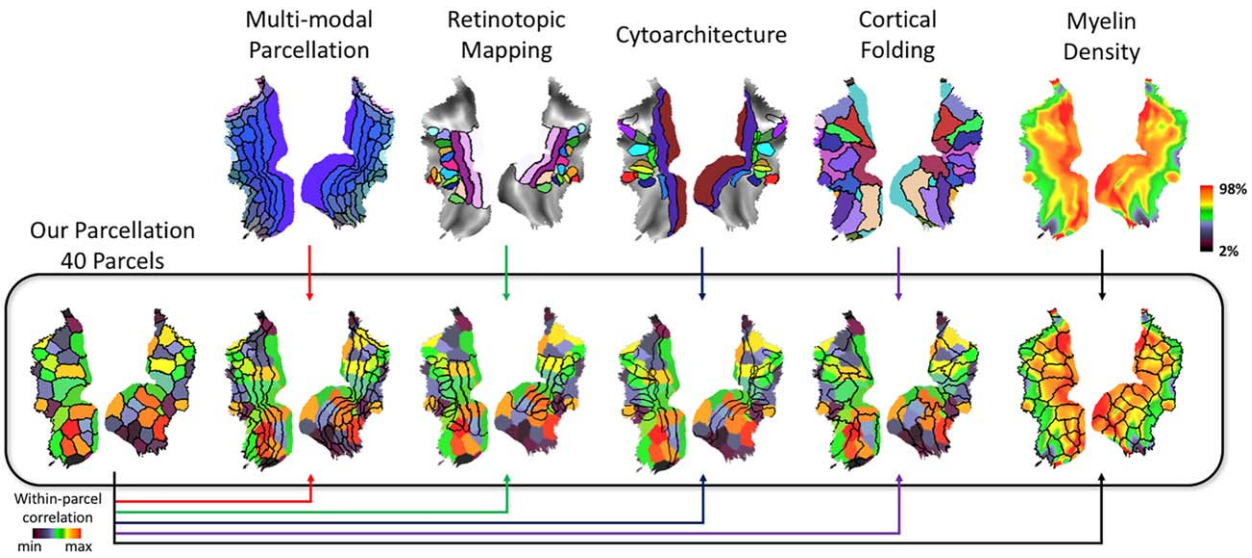

Figure 8.

Comparing our parcellation ($k = 40$) with existing visual cortex parcellations. Our functional parcellation is compared against (1) whole-brain multimodal images (i.e., MMP; Glasser et al., 2016); (2) visual-field maps (Abdollahi et al., 2014); (3) cytoarchitecture (Eickhoff et al., 2005); (4) cortical folding patterns (Destrieux et al., 2010); (5) cortical myelination (Glasser et al., 2014). The color vs. black arrows indicate the different sources of the underlay (black) versus overlap (color). With a color arrow, the functional parcellation obtained in this study is shown as the underlay, while an existing parcellation is shown as the overlay. With a black arrow, it is the opposite. [Color figure can be viewed at wileyonlinelibrary.com]

DISCUSSION

We characterized the network patterns emerging from spontaneous resting-state activity within the human visual cortex. On the basis of such patterns and their interactions, we delineated the intrinsic functional parcellation and organization of the visual cortex. Here, we report that fine-scale intrinsic visual cortical networks are not organized by the patterns of cortical retinotopy, folding, or cytoarchitecture, but align with the gradient of cortical myelination, and are segregated into functional modules specific to the ventral and dorsal visual streams.

Whole-Brain versus Fine-Scale Functional Networks

The majority of resting-state fMRI literature focuses on intrinsic functional networks in the whole brain scale (Smith et al., 2013). Large-scale networks are supported by long-range structural connections (Yeo et al., 2011), and are associated with coarsely defined functions (Smith et al., 2009). In a finer scale within the visual cortex, bi-directional structural connections co-exist over short distances (Felleman and Van Essen, 1991; Salin and Bullier, 1995), forming the network basis of vision (Rao and Ballard, 1999). The patterns and dynamics of fine-scale intrinsic networks may indicate how visual representations manifest themselves in spontaneous brain activity (Kenet et al., 2003), and offer a more specific clue on the functional role of spontaneous activity in shaping perception or behavior (Wilf et al., 2017).

To explore the topographic organization of fine-scale visual networks, it is necessary to confine the analysis to the functional connectivity profile within the visual system. Otherwise, in the whole-brain scale, the connectivity profile between a seed location in the visual cortex and the rest of the brain (as a function of locations) includes mostly the remote locations that are not or non-specifically associated with the seed location (or the "null" correlations). As a result, the difference in the whole-brain connectivity profile of two distinct seed locations becomes subtle, even if they may actually interact with different sets of brain locations in finer scales. Focusing on a fine scale improves the sensitivity to differentiate the topographic difference in functional connectivity of specific interest to vision. In line with this notion, previous studies have shown that fine-scale functional networks may be obscured by large-scale network activity (Raemaekers et al., 2014), and thus appear to exhibit a coarse topographic organization (Nir et al., 2006; Yeo et al., 2011).

ICA for Fine-Scale Functional Connectivity

Within the visual cortex, we used data-driven ICA to explore the multivariate voxel patterns and dynamics, instead of bivariate correlations between voxels or areas, as in previous studies (Arcaro et al., 2015; Bock et al., 2015; Butt et al., 2013; Dawson et al., 2016; Genc et al.,

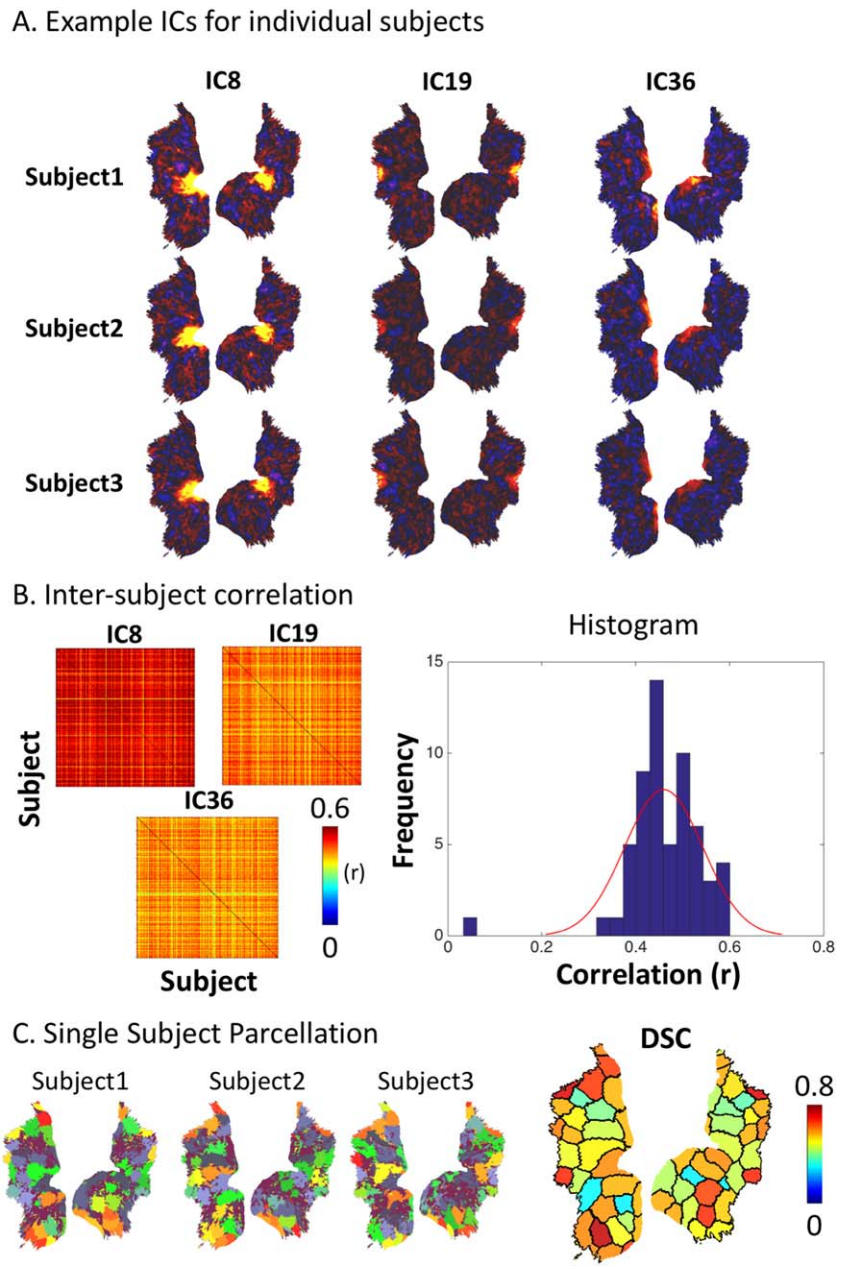

Figure 9.

ICs and parcellations from three individual subjects obtained through dual regression. **A**: Three example ICs from three subjects. **B**: The left panel shows the matrices of intersubject spatial cross-correlations (*r*). The right panel shows the histogram of intersubject correlations for all ICs, as well as its fitted distribution. **C**: The left shows the subject-wise parcellations obtained from three example subjects. The right shows the quantified overlap between individualized parcellations and the group-level parcellation. Each parcel is colored coded by the averaged DSC. [Color figure can be viewed at wileyonlinelibrary.com]

2016; de Zwart et al., 2013; Gravel et al., 2014; Heinzle et al., 2011; Raemaekers et al., 2014; Striem-Amit et al., 2015; Wilf et al., 2017; Yeo et al., 2011). In the whole-brain scale, ICA and seed-based correlation analyses have been shown to reveal similar network patterns (Van Dijk et al., 2010). However, structural connections are much denser at a reduced spatial scale or distance (Bassett and Bullmore, 2006), giving rise to more complex patterns of functional interactions. This makes ICA a more preferable method for fine-scale network mapping.

Our data suggest that RSNs within the visual cortex are robust in both group (Fig. 1) and individual (Fig. 9) levels, and are well-organized in both space (Figs. 2 through 4) and time (Figs. 5 and 6). In the group level, the reproducibility of ICA components was assessed based on back-to-back test and retest. An alternative and perhaps more indicative way to assess the reliability of fine-scale ICA may be based on longitudinal scans within the same subject, for example in (Poldrack et al., 2015). It should also be noted that reliable components are not necessarily of functional relevance or neuronal origin, since artifacts may also occur with reproducible patterns. One source of such artifacts – head motion, was taken into account in this study (Supporting Information Fig. S1). However, other artifacts, such as respiration and heart rate, are also of potential concern, and remain to be addressed in future studies.

Visual-Stream-Specific Modular Organization Persists after Discounting the Effect of Cortical Distance

Functional connectivity generally decays with increasing cortical distance not only in the whole-brain scale (Honey et al., 2009; Markov et al., 2012), but also in the fine-scale system (Genc et al., 2016). In other words, cortical locations that are closer to each other also tend to interact more with each other (Bassett and Bullmore, 2006; Das and Gilbert, 1999). In a trivial way, inter-voxel temporal correlations may also be affected by the point-spread function of BOLD fMRI (about 3–4 mm in 3T; Engel et al., 1997; Parkes et al., 2005). Although we recognize anatomical affinity as a non-trivial contributing factor to fine-scale functional connectivity, it is difficult to fully dissociate the effect of cortical distance on resting-state activity patterns. Future technical development is desirable to exclude the distance effect in ICA analysis.

In consideration of the distance dependence of fine-scale correlation patterns, one may argue that the observed modular organization within the visual cortex does not reflect true functional correlation but anatomical clustering. This argument is legitimate, since ventral and dorsal streams are both functionally and anatomically segregated. Results from this study suggest that the modular organization is not driven exclusively by anatomical affinity. After mathematically modeling and discounting the effect of cortical distance, the similar modular organization was still observed. The only difference was that after removing the cortical-distance effects, the dorsal module was divided into two modules: one mostly consisted of bilateral ICs (pink in Fig. 6G); the other mostly consisted of unilateral ICs (green in Fig. 6G). This difference likely resulted from the imperfect assumption of infinite inter-hemispherical distance, while neglecting another potential distance effect given the axonal connections between hemispheres. As such, the apparent subdivision of the dorsal module likely reflects a modeling effect, rather than any effect in functional organization. It should be also noted that functional connectivity exists between hemispheres or even appears negative occasionally. Neither of these could be explained by the geodesic cortical distance. In particular, inter-hemispherical correlation is a hallmark signature of functional connectivity in the whole brain, as well as in the visual cortex, especially for dorsal visual areas. In contrast, the anti-correlation within the visual cortex is not as common, but occurs without the global signal regression.

Fine-Scale Visual Networks Might Not Be Retinotopically Organized

However, unlike some prior studies (Gravel et al., 2014; Heinzle et al., 2011; Raemaekers et al., 2014), we did not find any evidence for the retinotopic organization of resting state activity beyond early visual areas. Perhaps, the exception was only in V1, where activity patterns were found to agree with eccentricity representations (Fig. 3A), consistent with previous findings (Arcaro et al., 2015; Wilf et al., 2017; Yeo et al., 2011). Beyond V1, spontaneous activity patterns were independent of either the eccentricity or the polar angle (Fig. 3). Even in V1, resting state activity was correlated between the left and right hemispheres (Fig. 3), although the two hemispheres correspond to different hemi-fields in the visual space. Note that the left and right V1 areas have little or no callosal connections (Tootell et al., 1998) to directly support their synchronization. The inter-hemispherical V1 correlation is most likely due to a common input to both hemispheres. The topography of this common input seems retinotopically non-specific, at least in terms of the polar angle. Plausible sources of common input to both hemispheres are neuromodulators, for example, acetylcholine, that regulate cortical processing by broadcasting chemical messages to nearly the entire cortex (Angela and Dayan, 2005). Another alternative source is the feedback from higher-order areas, as discussed later.

Arguably, the eccentricity-dependent intrinsic activity patterns in V1 may be coincidental, and reflect the relative distributions of magnocellular (M) and parvocellular (P) projections that happen to vary with eccentricity. Previous studies have shown that P cells, relative to M cells, over-represent the central vision but under-represent the periphery in lateral geniculate nuclei (LGN) (Connolly and Van Essen, 1984; Schiller et al., 1990) and V1 (Azzopardi et al., 1999; Baseler and Sutter, 1997). The ratio between P and M projections to/from V1 notably decreases with eccentricity (Baseler and Sutter, 1997). Note that P and M pathways convey distinct visual attributes, but share the same retinotopic maps (Denison et al., 2014; Nassi and Callaway, 2009). Although the representation of the M-to-P ratio seems similar as the eccentricity representation in V1, the M-P pathways bear a different organization specific to visual streams as opposed to visual locations. Caution should be exercised when interpreting an eccentricity-dependent pattern alone as evidence for the retinotopic organization.

However, results in this study should not be taken as evidence against the role of retinotopy in the organization of the visual cortex. Retinotopy is definitely one of the primary principles for the anatomical and functional organization in the visual system. Nevertheless, findings reported herein suggest that retinotopy may not play the major role in defining the spontaneously emerging patterns of activity in the resting state. An alternative organization is elaborated as below.

Resting-State Activity Reflects Feedback Visual-Network Interactions

We further speculate that the common input to V1, which drives visual-stream specific resting-state activity, arises from top-down modulations through feedback connections. In the visual hierarchy (Felleman and Van Essen, 1991), the population receptive field becomes larger and less specific from lower to higher visual areas (Wandell et al., 2007), to progressively converge information in the visual space through feedforward connections. While the feedforward connections are retinotopically organized, the feedback corticocortical connections are not so (Salin and Bullier, 1995). Through feedback, the top-down modulations transfer information about a large or even the whole visual field to cortical locations with specific receptive fields (Salin and Bullier, 1995), driving network activity patterns away from being retinotopically specific. It is conceivable that the organization of feedback connections plays a defining role to RSNs within the visual cortex. This is because when feedforward pathways are not driven by fluctuating external inputs, feedback pathways are still modulated by the brain's intrinsic activity or mental state.

In addition, feedback connections in the visual system are generally separable by the ventral and dorsal pathways (Gilbert and Li, 2013; Salin and Bullier, 1995), functionally specialized for recognition and action, respectively (Goodale and Milner, 1992; Ungerleider and Haxby, 1994). Such a visual-stream-specific organization also applies to feedback connections from V1 to LGN (Briggs and Usrey, 2009). It lends support for our interpretation that feedback projections serve the structural network basis of the observed modular organization of intrinsic fine-scale functional networks distributed along the ventral and dorsal pathways (Fig. 5). As the ventral and dorsal pathways become intricate in early visual areas, fine-scale network patterns in V1/V2/V3 are split into functional modules due to the differential distributions of the M and P cells along the eccentricity division (Fig. 5).

Intrinsic Functional Parcellation of the Visual Cortex

On the basis of fine-scale resting-state activity patterns, the functional parcellation of the visual cortex appeared to be notably different from other parcellations based on cortical folding, retinotopy, and cytoarchitecture. The discrepancy with the cortical folding is perhaps reasonable, because the relationship between cortical morphology and functional organization is elusive and indirect, despite a developmental linkage likely between them as proposed elsewhere (Benson et al., 2012; Ronan and Fletcher, 2015). The discrepancy with visual field maps is perhaps also understandable, for the reasons elaborated in previous sections. In addition, the parcellation based on functional connectivity is applicable to all locations in the visual cortex, whereas the visual field is not mappable at all visual areas. For the apparently different parcellations based on regional cellular composition and inter-regional functional connectivity suggests a lack of one-to-one relationships between cell types and functional networks.

Our results show that the functional networks and parcels seem to align with the gradient of myelination (Fig. 8). We speculate that spontaneous activity shapes myelin density. It has been shown that electrical activity may promote myelination(Gibson et al., 2014), and that functional organization and cortical myelination may co-vary given plasticity (Fields, 2015; Hunt et al., 2016). Greater myelin density may imply greater functional specificity but less plasticity: early sensory areas are more functionally specific with greater myelination or less plasticity, whereas higher-order or multisensory areas are less functionally specific with less myelin density and more plasticity (Glasser et al., 2014).

It is also interesting to note the difference in lateralization for resting-state activity patterns at ventral vs. dorsal streams: the ventral stream is more lateralized, whereas the dorsal stream tends to be more bilateral. The implication of such a difference in lateralization remains obscure, but is likely due to the distinct functions of the two streams. The dorsal stream is in part for visual attention (Desimone and Duncan, 1995), which involves both hemispheres (Gotts et al., 2013). In contrast, the ventral stream is primarily for visual recognition, and object (e.g., face) representations are often stronger in one hemisphere relative to the other (Rossion et al., 2012). However, the above speculation is not readily applicable to the apparent difference in lateralization at early visual areas: V1 activity is bilateral, whereas V2 and V3 tend to be more lateralized (Fig. 3).

CONFLICT OF INTEREST

nothing to report.

REFERENCES

Abdollahi RO, Kolster H, Glasser MF, Robinson EC, Coalson TS, Dierker D, Jenkinson M, Van Essen DC, Orban GA (2014): Correspondences between retinotopic areas and myelin maps in human visual cortex. Neuroimage 99:509–524.

Amunts K, Malikovic A, Mohlberg H, Schormann T, Zilles K (2000): Brodmann's areas 17 and 18 brought into stereotaxic space-where and how variable? Neuroimage 11:66–84.

Angela JY, Dayan P (2005): Uncertainty, neuromodulation, and attention. Neuron 46:681–692.

Arcaro MJ, Honey CJ, Mruczek RE, Kastner S, Hasson U (2015): Widespread correlation patterns of fMRI signal across visual cortex reflect eccentricity organization. Elife 4.

Azzopardi P, Jones KE, Cowey A (1999): Uneven mapping of magnocellular and parvocellular projections from the lateral geniculate nucleus to the striate cortex in the macaque monkey. Vis Res 39:2179–2189.

Baldassano C, Iordan MC, Beck DM, Fei-Fei L (2012): Voxel-level functional connectivity using spatial regularization. Neuroimage 63:1099–1106.

Baldassano C, Beck DM, Fei-Fei L (2013): Differential connectivity within the Parahippocampal Place Area. Neuroimage 75: 228–237.

Baseler H, Sutter E (1997): M and P components of the VEP and their visual field distribution. Vis Res 37:675–690.

Bassett DS, Bullmore E (2006): Small-world brain networks. Neuroscientist 12:512–523.

Beckmann CF, Smith SM (2004): Probabilistic independent component analysis for functional magnetic resonance imaging. IEEE Trans Med Imaging 23:137–152.

Bell AJ, Sejnowski TJ (1995): An information-maximization approach to blind separation and blind deconvolution. Neural Comput 7:1129–1159.

Benson NC, Butt OH, Datta R, Radoeva PD, Brainard DH, Aguirre GK (2012): The retinotopic organization of striate cortex is well predicted by surface topology. Curr Biol 22:2081–2085.

Biswal B, Zerrin Yetkin F, Haughton VM, Hyde JS (1995): Functional connectivity in the motor cortex of resting human brain using echo-planar mri. Magn Reson Med 34:537–541.

Blondel VD, Guillaume JL, Lambiotte R, Lefebvre E (2008): Fast unfolding of communities in large networks. J Stat Mech-Theory Exp 2008:P10008.

Bock AS, Binda P, Benson NC, Bridge H, Watkins KE, Fine I (2015): Resting-State Retinotopic Organization in the Absence of Retinal Input and Visual Experience. J Neurosci 35: 12366–12382.

Briggs F, Usrey WM (2009): Parallel processing in the corticogeniculate pathway of the macaque monkey. Neuron 62:135–146.

Butt OH, Benson NC, Datta R, Aguirre GK (2013): The fine-scale functional correlation of striate cortex in sighted and blind people. J Neurosci 33:16209–16219.

Calhoun VD, Liu J, Adali T (2009): A review of group ICA for fMRI data and ICA for joint inference of imaging, genetic, and ERP data. Neuroimage 45:S163–S172.

Cole MW, Bassett DS, Power JD, Braver TS, Petersen SE (2014): Intrinsic and task-evoked network architectures of the human brain. Neuron 83:238–251.

Connolly M, Van Essen D (1984): The representation of the visual field in parvicellular and magnocellular layers of the lateral geniculate nucleus in the macaque monkey. J Comp Neurol 226:544–564.

Damoiseaux JS, Rombouts SA, Barkhof F, Scheltens P, Stam CJ, Smith SM, Beckmann CF (2006): Consistent resting-state networks across healthy subjects. Proc Natl Acad Sci USA 103: 13848–13853.

Das A, Gilbert CD (1999): Topography of contextual modulations mediated by short-range interactions in primary visual cortex. Nature 399:655–661.

Dawson DA, Lam J, Lewis LB, Carbonell F, Mendola JD, Shmuel A (2016): Partial Correlation-Based Retinotopically Organized Resting-State Functional Connectivity Within and Between Areas of the Visual Cortex Reflects More Than Cortical Distance. Brain Connect 6:57–75.

de Zwart JA, van Gelderen P, Liu Z, Duyn JH (2013): Independent sources of spontaneous BOLD fluctuation along the visual pathway. Brain Topogr 26:525–537.

Denison RN, Vu AT, Yacoub E, Feinberg DA, Silver MA (2014): Functional mapping of the magnocellular and parvocellular subdivisions of human LGN. Neuroimage 102 Pt 2:358–369.

Desimone R, Duncan J (1995): Neural mechanisms of selective visual attention. Annu Rev Neurosci 18:193–222.

Destrieux C, Fischl B, Dale A, Halgren E (2010): Automatic parcellation of human cortical gyri and sulci using standard anatomical nomenclature. Neuroimage 53:1–15.

Doucet G, Naveau M, Petit L, Delcroix N, Zago L, Crivello F, Jobard G, Tzourio-Mazoyer N, Mazoyer B, Mellet E, Joliot M (2011): Brain activity at rest: A multiscale hierarchical functional organization. J Neurophysiol 105:2753–2763.

Eickhoff SB, Stephan KE, Mohlberg H, Grefkes C, Fink GR, Amunts K, Zilles K (2005): A new SPM toolbox for combining probabilistic cytoarchitectonic maps and functional imaging data. Neuroimage 25:1325–1335.

Engel SA, Glover GH, Wandell BA (1997): Retinotopic organization in human visual cortex and the spatial precision of functional MRI. Cereb Cortex 7:181–192.

Felleman DJ, Van Essen DC (1991): Distributed hierarchical processing in the primate cerebral cortex. Cereb Cortex 1:1–47.

Fields RD (2015): A new mechanism of nervous system plasticity: Activity-dependent myelination. Nat Rev Neurosci 16:756–767.

Finn ES, Shen X, Scheinost D, Rosenberg MD, Huang J, Chun MM, Papademetris X, Constable RT (2015): Functional connectome fingerprinting: Identifying individuals using patterns of brain connectivity. Nat Neurosci 18:1664–1671.

Fischl B, Rajendran N, Busa E, Augustinack J, Hinds O, Yeo BT, Mohlberg H, Amunts K, Zilles K (2008): Cortical folding patterns and predicting cytoarchitecture. Cereb Cortex 18: 1973–1980.

Fox MD, Greicius M (2010): Clinical applications of resting state functional connectivity. Front Syst Neurosci 4:19.

Fox MD, Raichle ME (2007): Spontaneous fluctuations in brain activity observed with functional magnetic resonance imaging. Nat Rev Neurosci 8:700–711.

Fox MD, Corbetta M, Snyder AZ, Vincent JL, Raichle ME (2006): Spontaneous neuronal activity distinguishes human dorsal and ventral attention systems. Proc Natl Acad Sci USA 103: 10046–10051.

Genc E, Scholvinck ML, Bergmann J, Singer W, Kohler A (2016): Functional Connectivity Patterns of Visual Cortex Reflect its Anatomical Organization. Cereb Cortex 26:3719–3731.

Gibson EM, Purger D, Mount CW, Goldstein AK, Lin GL, Wood LS, Inema I, Miller SE, Bieri G, Zuchero JB, Barres BA, Woo PJ, Vogel H, Monje M (2014): Neuronal activity promotes oligodendrogenesis and adaptive myelination in the mammalian brain. Science 344:1252304.

Gilbert CD, Li W (2013): Top-down influences on visual processing. Nat Rev Neurosci 14:350–363.

Glasser MF, Van Essen DC (2011): Mapping human cortical areas in vivo based on myelin content as revealed by T1- and T2-weighted MRI. J Neurosci 31:11597–11616.

Glasser MF, Sotiropoulos SN, Wilson JA, Coalson TS, Fischl B, Andersson JL, Xu J, Jbabdi S, Webster M, Polimeni JR, Van Essen DC, Jenkinson M Consortium WU-MH (2013): The

minimal preprocessing pipelines for the Human Connectome Project. Neuroimage 80:105–124.
Glasser MF, Goyal MS, Preuss TM, Raichle ME, Van Essen DC (2014): Trends and properties of human cerebral cortex: Correlations with cortical myelin content. Neuroimage 93 Pt 2:165–175.
Glasser MF, Coalson TS, Robinson EC, Hacker CD, Harwell J, Yacoub E, Ugurbil K, Andersson J, Beckmann CF, Jenkinson M, Smith SM, Van Essen DC (2016): A multi-modal parcellation of human cerebral cortex. Nature 536:171–178.
Goodale MA, Milner AD (1992): Separate visual pathways for perception and action. Trends Neurosci 15:20–25.
Gotts SJ, Jo HJ, Wallace GL, Saad ZS, Cox RW, Martin A (2013): Two distinct forms of functional lateralization in the human brain. Proc Natl Acad Sci USA 110:E3435–E3444.
Gravel N, Harvey B, Nordhjem B, Haak KV, Dumoulin SO, Renken R, Curcic-Blake B, Cornelissen FW (2014): Cortical connective field estimates from resting state fMRI activity. Front Neurosci 8:339.
Greicius MD, Krasnow B, Reiss AL, Menon V (2003): Functional connectivity in the resting brain: a network analysis of the default mode hypothesis. Proc Natl Acad Sci USA 100:253–258.
Guclu U, van Gerven MA (2015): Deep Neural Networks Reveal a Gradient in the Complexity of Neural Representations across the Ventral Stream. J Neurosci 35:10005–10014.
Hasson U, Yang E, Vallines I, Heeger DJ, Rubin N (2008): A hierarchy of temporal receptive windows in human cortex. J Neurosci 28:2539–2550.
Heinzle J, Kahnt T, Haynes JD (2011): Topographically specific functional connectivity between visual field maps in the human brain. Neuroimage 56:1426–1436.
Honey C, Sporns O, Cammoun L, Gigandet X, Thiran J-P, Meuli R, Hagmann P (2009): Predicting human resting-state functional connectivity from structural connectivity. Proc Natl Acad Sci USA 106:2035–2040.
Honey CJ, Kotter R, Breakspear M, Sporns O (2007): Network structure of cerebral cortex shapes functional connectivity on multiple time scales. Proc Natl Acad Sci USA 104:10240–10245.
Hubel DH, Wiesel TN (1962): Receptive fields, binocular interaction and functional architecture in the cat's visual cortex. J Physiol 160:106–154.
Hunt BA, Tewarie PK, Mougin OE, Geades N, Jones DK, Singh KD, Morris PG, Gowland PA, Brookes MJ (2016): Relationships between cortical myeloarchitecture and electrophysiological networks. Proc Natl Acad Sci USA 113:13510–13515.
Hutchison RM, Womelsdorf T, Allen EA, Bandettini PA, Calhoun VD, Corbetta M, Della Penna S, Duyn JH, Glover GH, Gonzalez-Castillo J (2013): Dynamic functional connectivity: Promise, issues, and interpretations. Neuroimage 80:360–378.
Jo HJ, Saad ZS, Gotts SJ, Martin A, Cox RW (2012): Quantifying agreement between anatomical and functional interhemispheric correspondences in the resting brain. PloS One 7: e48847.
Kenet T, Bibitchkov D, Tsodyks M, Grinvald A, Arieli A (2003): Spontaneously emerging cortical representations of visual attributes. Nature 425:954–956.
Lewis CM, Bosman CA, Womelsdorf T, Fries P (2016): Stimulus-induced visual cortical networks are recapitulated by spontaneous local and interareal synchronization. Proc Natl Acad Sci USA 113:E606–E615.
Long X, Goltz D, Margulies DS, Nierhaus T, Villringer A (2014): Functional connectivity-based parcellation of the human sensorimotor cortex. Eur J Neurosci 39:1332–1342.
Markov NT, Ercsey-Ravasz M, Gomes AR, Lamy C, Magrou L, Vezoli J, Misery P, Falchier A, Quilodran R, Gariel M, Sallet J, Gamanut R, Huissoud C, Clavagnier S, Giroud P, Sappey-Marinier D, Barone P, Dehay C, Toroczkai Z, Knoblauch K, Van Essen DC, Kennedy H (2012): A weighted and directed interareal connectivity matrix for macaque cerebral cortex. Cereb Cortex 24:17–36.
Martin A (2007): The representation of object concepts in the brain. Annu Rev Psychol 58:25–45.
Nassi JJ, Callaway EM (2009): Parallel processing strategies of the primate visual system. Nat Rev Neurosci 10:360–372.
Nir Y, Hasson U, Levy I, Yeshurun Y, Malach R (2006): Widespread functional connectivity and fMRI fluctuations in human visual cortex in the absence of visual stimulation. Neuroimage 30:1313–1324.
Ohiorhenuan IE, Mechler F, Purpura KP, Schmid AM, Hu Q, Victor JD (2010): Sparse coding and high-order correlations in fine-scale cortical networks. Nature 466:617–621.
Parkes LM, Schwarzbach JV, Bouts AA, Pullens P, Kerskens CM, Norris DG (2005): Quantifying the spatial resolution of the gradient echo and spin echo BOLD response at 3 Tesla. Magn Reson Med 54:1465–1472.
Poldrack RA, Laumann TO, Koyejo O, Gregory B, Hover A, Chen M-Y, Gorgolewski KJ, Luci J, Joo SJ, Boyd RL (2015): Long-term neural and physiological phenotyping of a single human. Nat Commun 6.
Raemaekers M, Schellekens W, van Wezel RJ, Petridou N, Kristo G, Ramsey NF (2014): Patterns of resting state connectivity in human primary visual cortical areas: a 7T fMRI study. Neuroimage 84:911–921.
Rao RPN, Ballard DH (1999): Predictive coding in the visual cortex: A functional interpretation of some extra-classical receptive-field effects. Nat Neurosci 2:79–87.
Ronan L, Fletcher PC (2015): From genes to folds: A review of cortical gyrification theory. Brain Struct Funct 220:2475–2483.
Rossion B, Hanseeuw B, Dricot L (2012): Defining face perception areas in the human brain: A large-scale factorial fMRI face localizer analysis. Brain Cogn 79:138–157.
Rubinov M, Sporns O (2010): Complex network measures of brain connectivity: Uses and interpretations. Neuroimage 52:1059–1069.
Salin PA, Bullier J (1995): Corticocortical connections in the visual system: Structure and function. Physiol Rev 75:107–154.
Schiller PH, Logothetis NK, Charles ER (1990): Functions of the colour-opponent and broad-band channels of the visual system. Nature 343:68–70.
Seeley WW, Menon V, Schatzberg AF, Keller J, Glover GH, Kenna H, Reiss AL, Greicius MD (2007): Dissociable intrinsic connectivity networks for salience processing and executive control. J Neurosci 27:2349–2356.
Shen X, Tokoglu F, Papademetris X, Constable RT (2013): Groupwise whole-brain parcellation from resting-state fMRI data for network node identification. Neuroimage 82:403–415.
Smith SM, Fox PT, Miller KL, Glahn DC, Fox PM, Mackay CE, Filippini N, Watkins KE, Toro R, Laird AR, Beckmann CF (2009): Correspondence of the brain's functional architecture during activation and rest. Proc Natl Acad Sci USA 106: 13040–13045.
Smith SM, Vidaurre D, Beckmann CF, Glasser MF, Jenkinson M, Miller KL, Nichols TE, Robinson EC, Salimi-Khorshidi G, Woolrich MW, Barch DM, Ugurbil K, Van Essen DC (2013): Functional connectomics from resting-state fMRI. Trends Cogn Sci 17:666–682.

Striem-Amit E, Ovadia-Caro S, Caramazza A, Margulies DS, Villringer A, Amedi A (2015): Functional connectivity of visual cortex in the blind follows retinotopic organization principles. Brain 138:1679–1695.

Tavor I, Parker Jones O, Mars RB, Smith SM, Behrens TE, Jbabdi S (2016): Task-free MRI predicts individual differences in brain activity during task performance. Science 352:216–220.

Tootell RB, Mendola JD, Hadjikhani NK, Liu AK, Dale AM (1998): The representation of the ipsilateral visual field in human cerebral cortex. Proc Natl Acad Sci USA 95:818–824.

Ungerleider LG, Haxby JV (1994): 'What' and 'where' in the human brain. Curr Opin Neurobiol 4:157–165.

Van Den Heuvel MP, Mandl RC, Kahn RS, Pol H, Hilleke E (2009): Functionally linked resting-state networks reflect the underlying structural connectivity architecture of the human brain. Hum Brain Mapp 30:3127–3141.

Van Dijk KR, Hedden T, Venkataraman A, Evans KC, Lazar SW, Buckner RL (2010): Intrinsic functional connectivity as a tool for human connectomics: Theory, properties, and optimization. J Neurophysiol 103:297–321.

Van Essen DC, Glasser MF, Dierker DL, Harwell J, Coalson T (2012a): Parcellations and hemispheric asymmetries of human cerebral cortex analyzed on surface-based atlases. Cereb Cortex 22:2241–2262.

Van Essen DC, Ugurbil K, Auerbach E, Barch D, Behrens TE, Bucholz R, Chang A, Chen L, Corbetta M, Curtiss SW, Della Penna S, Feinberg D, Glasser MF, Harel N, Heath AC, Larson-Prior L, Marcus D, Michalareas G, Moeller S, Oostenveld R, Petersen SE, Prior F, Schlaggar BL, Smith SM, Snyder AZ, Xu J, Yacoub E, WU-Minn HCP Consortium (2012b): The Human Connectome Project: A data acquisition perspective. Neuroimage 62:2222–2231.

Van Essen DC, Smith SM, Barch DM, Behrens TE, Yacoub E, Ugurbil K; Consortium WU-MH. (2013): The WU-Minn Human Connectome Project: An overview. Neuroimage 80:62–79.

Wandell BA, Dumoulin SO, Brewer AA (2007): Visual field maps in human cortex. Neuron 56:366–383.

Wang Z, Chen LM, Negyessy L, Friedman RM, Mishra A, Gore JC, Roe AW (2013): The relationship of anatomical and functional connectivity to resting-state connectivity in primate somatosensory cortex. Neuron 78:1116–1126.

Wilf M, Strappini F, Golan T, Hahamy A, Harel M, Malach R (2017): Spontaneously Emerging Patterns in Human Visual Cortex Reflect Responses to Naturalistic Sensory Stimuli. Cereb Cortex 27:750–763.

Yamins DL, DiCarlo JJ (2016): Using goal-driven deep learning models to understand sensory cortex. Nat Neurosci 19: 356–365.

Yeo BT, Krienen FM, Sepulcre J, Sabuncu MR, Lashkari D, Hollinshead M, Roffman JL, Smoller JW, Zollei L, Polimeni JR, Fischl B, Liu H, Buckner RL (2011): The organization of the human cerebral cortex estimated by intrinsic functional connectivity. J Neurophysiol 106:1125–1165.

Yoshimura Y, Dantzker JL, Callaway EM (2005): Excitatory cortical neurons form fine-scale functional networks. Nature 433: 868–873.